

Domain Adaptation for Different Sensor Configurations in 3D Object Detection

Satoshi Tanaka^{*}, Kok Seang Tan^{*}, Isamu Yamashita
TIER IV, Inc

satoshi.tanaka@tier4.jp

Abstract

Recent advances in autonomous driving have underscored the importance of accurate 3D object detection, with LiDAR playing a central role due to its robustness under diverse visibility conditions. However, different vehicle platforms often deploy distinct sensor configurations, causing performance degradation when models trained on one configuration are applied to another because of shifts in the point cloud distribution. Prior work on multi-dataset training and domain adaptation for 3D object detection has largely addressed environmental domain gaps and density variation within a single LiDAR; in contrast, the domain gap for different sensor configurations remains largely unexplored. In this work, we address domain adaptation across different sensor configurations in 3D object detection. We propose two techniques: Downstream Fine-tuning (dataset-specific fine-tuning after multi-dataset training) and Partial Layer Fine-tuning (updating only a subset of layers to improve cross-configuration generalization). Using paired datasets collected in the same geographic region with multiple sensor configurations, we show that joint training with Downstream Fine-tuning and Partial Layer Fine-tuning consistently outperforms naive joint training for each configuration. Our findings provide a practical and scalable solution for adapting 3D object detection models to the diverse vehicle platforms.

1. Introduction

The rapid development of autonomous driving has emphasized the critical role of 3D object detection in understanding complex environments [6, 15]. Among various sensing modalities, LiDAR (Light Detection and Ranging) has emerged as a primary sensor for autonomous vehicles due to its ability to provide high-resolution distance information and maintain robustness in challenging visibility conditions. Unlike conventional 2D image-based detection, LiDAR-based 3D object detection enables precise estimation

of object positions, shapes, and categories in 3D space, offering richer spatial awareness. Importantly, autonomous vehicles are not limited to passenger cars [22, 36] — they also include diverse platforms such as buses [37, 54], trucks [21, 32], and last-mile delivery robots [16, 18]. Each platform often employs a distinct sensor configuration, which significantly affects the distribution, density, and coverage of the resulting point clouds. As a result, a 3D object detection model optimized for a particular sensor setup often suffers from severe performance degradation when applied to data collected with a different configuration. Given the real-world deployment of autonomous systems with heterogeneous sensor layouts, it is imperative to enhance the generalization ability of 3D detectors across varying sensor configurations.

To address domain shifts in other contexts, such as geographic or environmental changes, research in domain adaptation for 3D object detection has gained increasing attention [30]. However, prior work has largely overlooked the sensor-configuration-induced domain gap. In practice, the placement and number of LiDAR sensors differ substantially: for example, nuScenes features a single top-mounted LiDAR, while commercial bus platforms often adopt corner-mounted configurations to mitigate self-occlusion. Even within the same geographic region, these structural differences result in distinct point cloud characteristics, leading to sensor-specific domain gaps.

An alternative approach to improve generalization is multi-dataset training, in which multiple labeled datasets from different domains are jointly used for training. While this strategy can produce robust models, it often leads to trade-offs in per-dataset performance due to overgeneralization — a phenomenon reminiscent of the No Free Lunch theorem. Notably, in many robotics applications, especially those deployed in fixed environments, it is acceptable to deploy per-configuration models rather than enforce full generalization across all sensor types. Despite this practical relevance, research specifically aimed at obtaining high-performing models for each sensor configuration remains limited.

Motivated by this domain gap, we investigate domain

^{*}Equal contribution

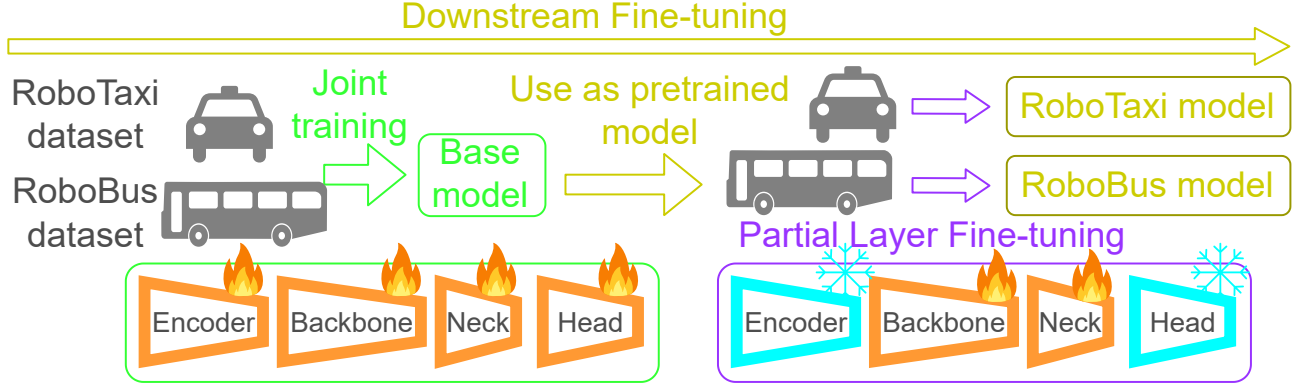


Figure 1. Overview of the proposed training strategy combining Downstream Fine-tuning and Partial Layer Fine-tuning, as our concept of domain adaptation for different sensor configurations. Downstream Fine-tuning improves performance by first jointly training on all sensor configurations to learn generalizable features, then fine-tuning each configuration to specialize to its characteristics. Partial Layer Fine-tuning improves performance by selectively updating layers most sensitive to sensor-configuration shifts — training the backbone and neck while freezing the encoder and head — to adapt spatial features.

adaptation for 3D object detection across different sensor configurations. An overview of our proposed framework is presented in Figure 1. We introduce two adaptation techniques: Downstream Fine-tuning and Partial Layer Fine-tuning. Downstream Fine-tuning adopts a two-stage training strategy, where a model is initially trained on multiple datasets and subsequently fine-tuned separately on each dataset. Partial Layer Fine-tuning updates only a subset of layers, enabling efficient and configuration-specific adaptation. To support our experiments, we construct a dataset comprising sensor configurations for both RoboTaxi and RoboBus, collected within the same geographic region. We evaluate the proposed methods under both sensor configuration settings. Specifically, we make three key contributions:

- We construct a dataset featuring different sensor configurations that share a common annotation specification, collected within the same geographic domain, to analyze the domain gap introduced by sensor variation.
- We propose a supervised training pipeline combining Downstream Fine-tuning and Partial Layer Fine-tuning to adapt 3D detectors for each sensor configuration individually.
- We construct a new multi-configuration 3D detection benchmark with different sensor setups, and provide a thorough quantitative evaluation.

2. Background

LiDAR-based 3D object detection. For a long time, researchers have developed 3D object detection models using LiDAR point clouds [23–26, 43, 47]. VoxelNet [53] introduces a voxel-based end-to-end pipeline for 3D object detection from point clouds. SECOND [42] improves voxel-based 3D object detection by introducing sparse 3D

	KITTI	ONCE	nuScenes	Waymo
Single dataset	47.4	60.2	18.4	40.2
MDT3D [28]	41.8	38.2	11.0	6.4

Table 1. Multi-dataset training underperforms compared to models trained on each single dataset individually.

	UDA, SSDA	TTA	MDT	Ours
Annotation configuration	Different	Different	Different	Same
Sensor configuration	Similar	Similar	Similar	Different
Source data	$\{x^s, y^s\}$	None	$\{x^s, y^s\}$	$\{x^s, y^s\}$
Target data	$\{x^t\} (+\{y^t\})$	x^t	$\{x^t, y^t\}$	$\{x^t, y^t\}$
Improve for target data?	Yes	Yes	Yes	Yes
Improve for source data?	No	No	Yes	Yes

Table 2. Method comparison between unsupervised domain adaptation (UDA), Semi-supervised domain adaptation (SSDA), Test-time adaptation (TTA), and multi-dataset training (MDT).

convolutions, enabling more efficient and scalable processing of large point clouds. PointPillars [11] encodes point clouds into a pseudo-image using pillar-based representations. CenterPoint [48] formulates 3D object detection as a center point prediction task, enabling accurate and efficient localization of objects in point clouds. TransFusion [3] introduces an attention-based framework for the head of 3D object detection, improving performance by multi-modal features.

Datasets for 3D domain adaptation. There are several datasets commonly used in research on domain adaptation for 3D object detection. The KITTI dataset [8] was collected in Germany using a 64-beam LiDAR sensor, and contains annotations for 3 classes with a front-view-only. The nuScenes dataset [5] was collected in the USA and Singapore using a 32-beam LiDAR sensor, and provides

360-degree annotations for 10 classes. The Waymo Open Dataset [29] was collected in the USA using a 64-beam LiDAR sensor, and includes 360-degree annotations for 5 classes. The ONCE dataset [14] was collected in China using a 40-beam LiDAR sensor, and contains 360-degree annotations for 9 classes. These datasets were acquired with a primary LiDAR sensor on the top of a passenger car.

Domain adaptation for 3D object detection.

Researchers have tackled this problem as an unsupervised domain adaptation (UDA) task using open datasets [12, 31, 34, 40, 41, 45, 46]. ST3D [45] performs unsupervised domain adaptation for 3D object detection via progressive self-training with pseudo-labels. ST3D++ [46] enhances ST3D by applying denoising strategies to improve pseudo-labels in unsupervised domain adaptation for 3D object detection. Several studies have focused on the differences in object distributions across domains [13, 33, 51]. Other studies have also focused on differences in LiDAR sensor characteristics, such as the number of channels in mechanical LiDARs and variations across sensor models [7, 9, 20, 38]. Semi-supervised domain adaptation (SSDA) for 3D object detection has also been explored to address the domain gap using a small amount of annotated target data and unlabeled data [10, 34, 49]. Test-time adaptation (TTA) for 3D object detection aims to improve 3D object detection without requiring source data or additional annotations [50]. It enhances bounding box regression through consistency regularization and adaptive optimization during inference.

The framework of multi-dataset training (MDT) for 3D object detection also aims to achieve greater generalization across diverse domains [28, 35, 39]. However, as summarized by the experimental results of MDT3D [28] using CenterPoint in Table 1, show that although training on all datasets jointly improves generalization, it often leads to lower performance on individual datasets compared to models trained solely on those datasets. This reflects a well-known issue as No Free Lunch theorem. When the goal is to maximize performance on a specific dataset, which is often the case in industry applications, such joint training may actually degrade performance.

While prior work has advanced, few studies have addressed performance degradation caused by sensor configuration differences. Most studies use open datasets with differing annotation schemes, focusing on domain gaps in labeling or object size, and often on the number of beams in a single LiDAR. To our knowledge, this is the first work to directly target the performance impact of sensor placement differences between single- and multi-LiDAR setups, under a unified annotation format. We summarize the related work in Table 2.

3. Method

3.1. Multi-sensor configuration dataset

As illustrated in Figure 2 (a), we constructed a multi-configuration dataset with a consistent annotation format across different sensor setups. The dataset includes two representative LiDAR configurations inspired by real-world autonomous vehicle platforms: RoboTaxi and RoboBus. The RoboTaxi configuration reflects a typical sensor layout for autonomous passenger cars. It consists of a single top-mounted LiDAR and several surrounding sub LiDARs positioned to minimize blind spots. All LiDAR point clouds are concatenated and used as the model input. In our setup, the top LiDAR is a 128-beam sensor, and the sub LiDARs are 16-beam sensors. This configuration closely resembles existing datasets such as nuScenes. The RoboBus configuration, in contrast, reflects the sensor layout for autonomous buses. It includes LiDARs placed at the front, rear, and front corners of the vehicle. This configuration is necessary for large, box-shaped vehicles like buses, where a single roof-mounted LiDAR would leave substantial blind spots along the lower side and rear areas. The RoboBus configuration includes multiple 40-beam main LiDARs and multiple 64-beam short-range LiDARs. All data for the RoboTaxi and RoboBus datasets were collected in both urban and suburban environments in Japan. The RoboTaxi dataset contains about 21,000 frames, and the RoboBus dataset about 13,000 frames. The annotation schema consists of five classes: Car, Truck, Bus, Bicycle, and Pedestrian. To the best of our knowledge, this is the first work to construct and experimentally evaluate datasets with different sensor configurations under a unified annotation standard within the same country.

3.2. Training pipeline

Whole architecture for supervised learning. Figure 1 illustrates the overall architecture for supervised learning. As the overall training pipeline, we adopt a multi-stage learning strategy based on Downstream Fine-tuning. For fine-tuning with each sensor configuration, we apply Partial Layer Fine-tuning. By incorporating these approaches, we obtain models that are optimally tuned for each specific sensor configuration.

Whole architecture for unsupervised learning. In this study, we also develop an unsupervised domain adaptation pipeline to analyze the domain gap caused by differences in sensor configurations. Figure 2 (b) illustrates the overall architecture for unsupervised learning. As the overall training pipeline, we fine-tune using pseudo-labels generated by an offline model, which uses a more computationally intensive algorithm and larger model parameters to achieve higher performance.

Downstream Fine-tuning for Different Sensor Con-

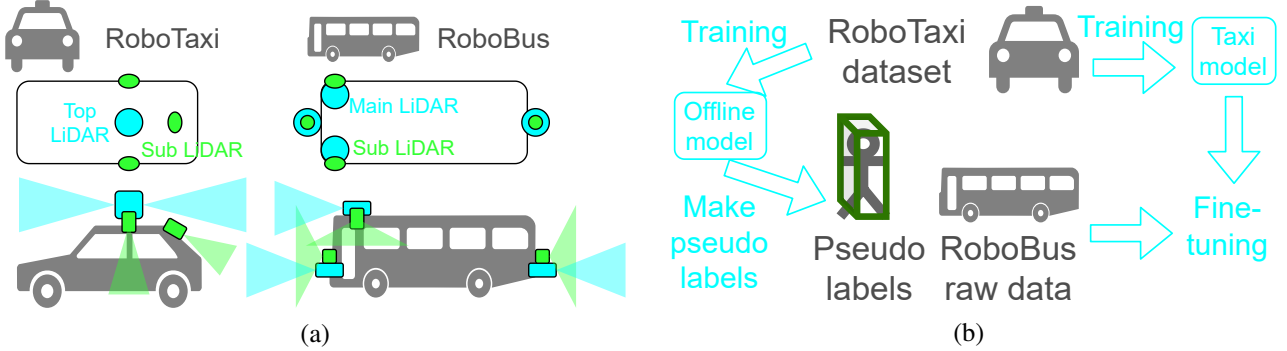


Figure 2. (a) Multi-configuration dataset with a consistent annotation format across different sensor setups. The dataset includes RoboTaxi and RoboBus configurations, reflecting real-world autonomous vehicle platforms with distinct LiDAR layouts, collected across urban and suburban areas in Japan. (b) Overview of the unsupervised domain adaptation pipeline to analyze domain gaps from different sensor configurations. Pseudo-labels generated by a high-capacity offline model are used to fine-tune the model for a target sensor configuration.

figurations. To improve performance for each sensor configuration, we adopt a Downstream Fine-tuning approach as part of a multi-stage training strategy. First, we perform joint training using all available data across different sensor configurations. This stage aims to learn generalizable representations and improve robustness across domains. Subsequently, we apply fine-tuning on each individual sensor configuration dataset to adapt the model to specific domain characteristics. This step enables the model to specialize in the unique features and distributions of each configuration.

Partial Layer Fine-tuning. To improve efficiency and performance, we employ Partial Layer Fine-tuning, selectively updating only the layers most effective at bridging domain gaps. Specifically, we identify and fine-tune layers that are sensitive to differences in sensor configurations, while freezing the remaining layers to reduce computational cost and prevent overfitting. This approach enables efficient adaptation to domain-specific features. Recent LiDAR-based 3D object detection models are typically composed of four key modules: encoder, backbone, neck, and head. In general, the encoder is influenced by input-level properties such as point cloud distribution and intensity patterns. The head, on the other hand, is affected by output-level characteristics, including object size and annotation formats, as it directly predicts detection targets. The backbone and neck serve to extract spatial features, and are thus sensitive to viewpoint and sensor placement. Based on these characteristics, we adopt the following strategy in our setup as detailed in the Appendix. Since the same mechanical LiDAR is used across configurations and both utilize concatenated point clouds, the encoder experiences similar input distributions and is therefore kept fixed. In contrast, as sensor layouts differ between configurations, the spatial features extracted by the backbone and neck must adapt accordingly; thus, we make these modules trainable. Finally, since the annotation protocol is consistent and the nature of

the objects to be detected remains the same, the head is also fixed.

4. Experiment

4.1. Setting

We used CenterPoint as the 3D object detection model throughout all experiments. Our CenterPoint consists of encoder of PointPillars [11] as encoder, SECOND [42] as backbone, FPN of SECOND [42] as neck, and head of CenterPoint [48] as head. Voxel size is 0.32 m and we do not use multi-frame input (densification). We conduct experiments on the multi-sensor configuration dataset as described in Section 3.1 and split train, val, and test data for each sensor configuration. The detection and inference range was set to 120 m. For evaluation, we followed the same mAP definition as the nuScenes benchmark. For the experiments of unsupervised learning, we use the LiDAR-only version of TransFusion [3] as the offline model. Voxel size of the offline model is 0.075 m and we do not use multi-frame input.

4.2. Result

Tables 3 (a) and (b) summarize the evaluation results for supervised learning across different combinations of sensor configurations and the use of fine-tuning. In Table 3 (a), training with only the RoboTaxi dataset yields a baseline mAP of 58.6. Incorporating additional data from the RoboBus configuration improves performance to 63.3, demonstrating the benefit of multi-configuration training. Applying fine-tuning further enhances the mAP to 64.7, with notable gains in the Bus and Bicycle classes, indicating improved cross-domain generalization. Similarly, in Table 3 (b), training with only the RoboBus configuration results in an mAP of 62.0. When both RoboTaxi and RoboBus datasets are used, the mAP increases to 64.5. With fine-

Table 3. The evaluation summary of (a) RoboTaxi dataset and (b) RoboBus dataset. "RT." means using RoboTaxi dataset. "RB." means using RoboBus dataset. "FT." means our fine-tuning methods. "Tru." means truck. "Bic." means bicycle. "Ped." means pedestrian.

RT.	RB.	FT.	mAP	Car	Tru.	Bus	Bic.	Ped.
✓			58.6	74.8	52.8	49.7	50.0	67.6
✓	✓		63.3	74.8	53.3	66.4	56.3	65.5
✓	✓	✓	64.7	75.3	50.4	70.0	62.8	65.0

(a)

RT.	RB.	FT.	mAP	Car	Tru.	Bus	Bic.	Ped.
	✓		62.0	82.9	59.8	57.5	60.0	49.8
✓	✓		64.5	75.0	45.5	86.6	51.2	63.9
✓	✓	✓	65.6	75.5	46.4	89.5	54.0	62.6

(b)

Table 4. Ablation study of Partial Layer Fine-tuning. (a) Fine-tuning for RoboTaxi dataset. (b) Fine-tuning for RoboBus dataset. "En." means encoder. "Ba." means backbone. "Ne." means neck. "He." means head.

En.	Ba.	Ne.	He.	mAP	Car	Tru.	Bus	Bic.	Ped.
				63.3	74.8	53.3	66.4	56.3	65.5
			✓	63.2	74.9	52.2	66.6	56.7	65.7
	✓			64.0	75.4	50.3	69.7	59.2	65.5
✓	✓			64.6	75.3	50.7	70.6	61.2	65.4
✓	✓	✓		64.3	75.3	50.7	71.6	58.2	65.6
	✓	✓		64.7	75.3	50.4	70.0	62.8	65.0
	✓	✓	✓	64.2	75.0	50.0	70.8	60.0	65.1
✓	✓	✓	✓	64.1	75.3	50.5	70.1	58.4	65.9

(a)

En.	Ba.	Ne.	He.	mAP	Car	Tru.	Bus	Bic.	Ped.
				64.5	75.0	45.5	86.6	51.2	63.9
			✓	63.2	75.2	42.2	85.9	50.0	62.6
	✓			65.4	75.1	46.4	90.4	52.6	62.6
✓	✓			65.3	75.3	46.8	88.1	54.1	62.2
✓	✓	✓		64.8	75.7	45.7	87.9	52.6	62.3
	✓	✓		65.6	75.5	46.4	89.5	54.0	62.6
	✓	✓	✓	65.2	75.1	46.5	88.0	54.7	61.9
✓	✓	✓	✓	65.1	75.7	45.9	87.9	54.4	61.9

(b)

tuning, performance improves further to 65.6, achieving the best results overall. The most significant improvements are observed in the Bus and Bicycle categories, which are likely more affected by domain shift across sensor setups. These results confirm that incorporating data from multiple sensor configurations contributes to better generalization, and that fine-tuning effectively adapts the model to diverse domains, leading to consistent performance improvements across classes. The transition from training on RoboBus only to training on both datasets exhibits a larger performance gap compared to the transition from RoboTaxi only to both datasets. This discrepancy can be attributed to the greater number of frames in the RoboTaxi dataset, which causes the jointly trained base model to be more heavily influenced by the sensor configuration domain of RoboTaxi. Our results demonstrate that this RoboTaxi-biased representation can be partially mitigated through downstream fine-tuning, allowing the model to better adapt to the characteristics of other sensor configurations such as RoboBus.

4.3. Analysis

Table 4 presents an ablation study of our Partial Layer Fine-tuning method on the RoboTaxi (a) and RoboBus (b) datasets. We incrementally enable fine-tuning for different modules — encoder, backbone, neck, and head — to assess their individual and combined contributions. In both settings, fine-tuning only the head slightly degrades performance compared to no fine-tuning, suggesting that isolated tuning of output layers is insufficient for different sensor configuration. Tuning the backbone leads to improvements,

and additional tuning of the encoder and neck further boosts performance. Interestingly, tuning all modules does not always yield the best result. The highest mAP on RoboTaxi and RoboBus is achieved when fine-tuning the backbone and neck only, highlighting that selective adaptation of specific layers is more effective than full fine-tuning. These results support the effectiveness of our partial tuning strategy in balancing adaptation performance with parameter efficiency. They also demonstrate that naive fine-tuning is not sufficient to achieve optimal performance, whereas Partial Layer Fine-tuning provides a more effective means of adapting to different sensor configurations.

Table 5 presents the evaluation results under various training conditions and fine-tuning settings across different combinations of sensor configurations. The model trained only on RoboTaxi performs poorly when evaluated on RoboBus, achieving an mAP of just 53.1. This performance drop is particularly severe in the Bus (36.4) and Truck (45.0) classes, highlighting a substantial domain gap caused by the differences in sensor configurations between RoboTaxi and RoboBus. To address this issue, we gradually applied fine-tuning using different portions of RoboBus data. Interestingly, using only 10% of RoboBus data raised the mAP significantly to 61.8, with the Bus class improving dramatically to 70.9. As the amount of fine-tuning data increased, performance continued to improve, reaching an mAP of 64.6 when using 100% of the data, matching the result obtained by joint training. These results suggest that fine-tuning alone, without the source-domain dataset, can achieve performance comparable to joint training for dif-

Table 5. The evaluation results for RoboBus dataset under various training condition and fine-tuning settings. "DS." means Downstream Fine-tuning. "PL." means Partial Layer Fine-tuning.

Condition	DS.	PL.	mAP	Car	Tru.	Bus	Bic.	Ped.
RoboTaxi			53.1	72.0	45.0	36.4	46.9	65.0
RoboTaxi → Fine-tuning by RoboBus (10%)			61.8	73.7	46.7	70.9	53.2	64.5
RoboTaxi → Fine-tuning by RoboBus (20%)			62.9	74.1	48.4	74.4	52.6	65.1
RoboTaxi → Fine-tuning by RoboBus (50%)			63.4	74.3	46.0	78.0	54.3	64.7
RoboTaxi → Fine-tuning by RoboBus (100%)			64.6	74.6	45.9	82.1	55.8	64.6
Joint training			64.5	75.0	45.5	86.6	51.2	63.9
Joint training → Fine-tuning by RoboBus	✓		65.1	75.7	45.9	87.9	54.4	61.9
Joint training → Fine-tuning by RoboBus	✓	✓	65.6	75.5	46.4	89.5	54.0	62.6

Table 6. The evaluation results under unsupervised learning domain adaptation to analyze the domain gap. "PL." means Partial Layer Fine-tuning. In this experiment, we use pseudo-labels for the RoboBus dataset generated from unlabeled RoboBus data.

Condition	PL.	mAP	Car	Tru.	Bus	Bic.	Ped.
RoboTaxi		53.1	72.0	45.0	36.4	46.9	65.0
Joint training		64.5	75.0	45.5	86.6	51.2	63.9
RoboTaxi → Fine-tuning by Pseudo-labeled RoboBus		52.0	72.0	46.1	40.5	42.6	58.6
RoboTaxi → Fine-tuning by Pseudo-labeled RoboBus	✓	52.3	72.4	46.7	39.2	44.7	58.2

ferent sensor configurations. For the models trained via joint training, we further applied downstream fine-tuning, which improved the mAP from 64.5 to 65.1, surpassing models fine-tuned from the RoboTaxi-only baseline. Moreover, applying our Partial Layer Fine-tuning method further improved performance to 65.6 mAP. These findings demonstrate the effectiveness of our fine-tuning strategy, particularly in adapting to sensor-specific domain shifts.

To further investigate the domain gap between different sensor configurations, we conducted an experiment on unsupervised domain adaptation using pseudo-labels generated from the RoboBus dataset without annotations. Table 6 presents the evaluation results under this setting. When fine-tuning the RoboTaxi model with pseudo-labeled RoboBus data (RoboTaxi → Fine-tuning by Pseudo-labeled RoboBus), the mAP decreased slightly to 52.0. To mitigate this, we applied Partial Layer Fine-tuning, aiming to avoid overfitting to potentially inaccurate pseudo-labels, and this adjustment led to a minor improvement, raising mAP to 52.3. Despite this marginal gain, the results remain significantly lower than the RoboTaxi model. Although the performance of Truck (45.0 → 46.7) and Bus (36.4 → 39.2) slightly improves under the pseudo-label setting, we observe a decline in performance for smaller objects such as Bicycle (46.9 → 44.7) and Pedestrian (65.0 → 58.2). This suggests that generating accurate pseudo-labels for small objects is particularly challenging, likely due to the limitations of the offline model used for pseudo-labeling. As noted in [50], the mAP for three-class domain adaptation from Waymo to nuScenes under an unsupervised setting remains in the teens. This highlights how unsupervised domain adaptation on public datasets tends to produce low

baseline results, framing it more as a detection or discovery task ("can we find the objects?"). In contrast, the domain gap caused by sensor configuration differences is comparatively narrower. The focus here shifts beyond simple detection to improving localization and classification accuracy — in other words, from finding to refining. This distinction supports the motivation behind our fine-tuning strategy, which aims not merely to enable detection in a new domain, but to enhance detection quality by adapting to sensor-specific characteristics. The results reinforce that our approach to refine for sensor configuration by fine-tuning is well-suited to this refinement phase of domain adaptation.

5. Conclusion

In this paper, we addressed domain adaptation in 3D object detection under varying LiDAR sensor configurations. To address this, we proposed a fine-tuning framework combining Downstream Fine-tuning and Partial Layer Fine-tuning, enabling efficient adaptation to each sensor setup. We constructed a unified multi-configuration dataset and demonstrated through fine-tuning experiments that our method improves per-configuration performance over joint training. Ablation studies further highlight that partial fine-tuning offers a better balance between accuracy and efficiency than full model tuning. Our unsupervised domain adaptation experiments demonstrate that fine-tuning for sensor-specific configurations effectively addresses the narrower domain gap. We believe this work contributes to making 3D object detectors more adaptable to real-world vehicle platform diversity, helping support broader deployment of autonomous driving systems.

References

- [1] Llama Team at Meta. Llama 2: Open foundation and fine-tuned chat models, 2023. 1
- [2] Llama Team at Meta. The llama 3 herd of models, 2024. 1
- [3] Xuyang Bai, Zeyu Hu, Xinge Zhu, Qingqiu Huang, Yilun Chen, Hongbo Fu, and Chiew-Lan Tai. Transfusion: Robust lidar-camera fusion for 3d object detection with transformers. *2022 IEEE/CVF Conference on Computer Vision and Pattern Recognition (CVPR)*, pages 1080–1089, 2022. 2, 4
- [4] Tom B. Brown, Benjamin Mann, Nick Ryder, Melanie Subbiah, Jared Kaplan, Prafulla Dhariwal, Arvind Neelakantan, Pranav Shyam, Girish Sastry, Amanda Askell, Sandhini Agarwal, Ariel Herbert-Voss, Gretchen Krueger, Tom Henighan, Rewon Child, Aditya Ramesh, Daniel M. Ziegler, Jeffrey Wu, Clemens Winter, Christopher Hesse, Mark Chen, Eric Sigler, Mateusz Litwin, Scott Gray, Benjamin Chess, Jack Clark, Christopher Berner, Sam McCandlish, Alec Radford, Ilya Sutskever, and Dario Amodei. Language models are few-shot learners, 2020. 1
- [5] Holger Caesar, Varun Bankiti, Alex H. Lang, Sourabh Vora, Venice Erin Liong, Qiang Xu, Anush Krishnan, Yu Pan, Giancarlo Baldan, and Oscar Beijbom. nuscenes: A multi-modal dataset for autonomous driving. In *CVPR*, 2020. 2
- [6] Siheng Chen, Baoan Liu, Chen Feng, Carlos Vallespi-Gonzalez, and Carl K. Wellington. 3d point cloud processing and learning for autonomous driving: Impacting map creation, localization, and perception. *IEEE Signal Processing Magazine*, 38:68–86, 2020. 1
- [7] Jinhao Deng, Wei Ye, Hai Wu, Xun Huang, Qiming Xia, Xin Li, Jin Fang, Wei Li, Chenglu Wen, and Cheng Wang. Cmd: A cross mechanism domain adaptation dataset for 3d object detection. In *Computer Vision – ECCV 2024*, pages 219–236. Springer, 2024. 3
- [8] Andreas Geiger, Philip Lenz, and Raquel Urtasun. Are we ready for autonomous driving? the kitti vision benchmark suite. In *Conference on Computer Vision and Pattern Recognition (CVPR)*, 2012. 2
- [9] Qianjiang Hu, Daizong Liu, and Wei Hu. Density-insensitive unsupervised domain adaption on 3d object detection. In *Proceedings of the IEEE/CVF Conference on Computer Vision and Pattern Recognition (CVPR)*, 2023. 3
- [10] Yecheol Kim, Junho Lee, Changsoo Park, Hyoung won Kim, Inho Lim, Christopher Chang, and Jun Won Choi. Semi-supervised domain adaptation using target-oriented domain augmentation for 3d object detection. *IEEE Transactions on Intelligent Vehicles*, pages 1–12, 2024. 3
- [11] Alex H. Lang, Sourabh Vora, Holger Caesar, Lubing Zhou, Jiong Yang, and Oscar Beijbom. Pointpillars: Fast encoders for object detection from point clouds. *2019 IEEE/CVF Conference on Computer Vision and Pattern Recognition (CVPR)*, pages 12689–12697, 2018. 2, 4
- [12] Shuangzhi Li, Lei Ma, and Xingyu Li. Domain generalization of 3d object detection by density-resampling. In *European Conference on Computer Vision*, pages 456–473. Springer, 2024. 3
- [13] Xiaohu Lu and Hayder Radha. Dali: Domain adaptive lidar object detection via distribution-level and instance-level pseudo label denoising. *IEEE Transactions on Robotics*, 2024. 3
- [14] Jiageng Mao, Minzhe Niu, Chenhan Jiang, Xiaodan Liang, Yamin Li, Chaoqiang Ye, Wei Zhang, Zhenguo Li, Jie Yu, Chunjing Xu, et al. One million scenes for autonomous driving: Once dataset. 2021. 3
- [15] Jiageng Mao, Shaoshuai Shi, Xiaogang Wang, and Hongsheng Li. 3d object detection for autonomous driving: A comprehensive survey, 2023. 1
- [16] Meituan Inc. Meituan: Autonomous delivery and urban service platform. <https://about.meituan.com/en>, 2025. Accessed: 2025-05-09. 1
- [17] Shervin Minaee, Tomas Mikolov, Narjes Nikzad, Meysam Chenaghlu, Richard Socher, Xavier Amatriain, and Jianfeng Gao. Large language models: A survey, 2025. 1
- [18] Nuro, Inc. Nuro: Autonomous delivery for everyday needs. <https://www.nuro.ai/>, 2025. Accessed: 2025-05-09. 1
- [19] OpenAI. Gpt-4 technical report, 2024. 1
- [20] Xidong Peng, Xinge Zhu, and Yuexin Ma. Cl3d: Unsupervised domain adaptation for cross-lidar 3d detection. In *Proceedings of the AAAI Conference on Artificial Intelligence*, pages 2047–2055, 2023. 3
- [21] Plus, Inc. Plus: Transforming the trucking industry with self-driving technology. <https://www.plus.ai/>, 2025. Accessed: 2025-05-10. 1
- [22] Pony.ai, Inc. Pony.ai: Autonomous driving technology. <https://www.pony.ai/>, 2025. Accessed: 2025-05-09. 1
- [23] C. Qi, Hao Su, Kaichun Mo, and Leonidas J. Guibas. Pointnet: Deep learning on point sets for 3d classification and segmentation. *2017 IEEE Conference on Computer Vision and Pattern Recognition (CVPR)*, pages 77–85, 2016. 2
- [24] Charles R. Qi, Li Yi, Hao Su, and Leonidas J. Guibas. Pointnet++: deep hierarchical feature learning on point sets in a metric space. In *Proceedings of the 31st International Conference on Neural Information Processing Systems*, page 5105–5114, Red Hook, NY, USA, 2017. Curran Associates Inc.
- [25] Shaoshuai Shi, Xiaogang Wang, and Hongsheng Li. Pointnet-cnn: 3d object proposal generation and detection from point cloud. *2019 IEEE/CVF Conference on Computer Vision and Pattern Recognition (CVPR)*, pages 770–779, 2018.
- [26] Shaoshuai Shi, Chaoxu Guo, Li Jiang, Zhe Wang, Jianping Shi, Xiaogang Wang, and Hongsheng Li. Pv-rcnn: Point-voxel feature set abstraction for 3d object detection. *2020 IEEE/CVF Conference on Computer Vision and Pattern Recognition (CVPR)*, pages 10526–10535, 2019. 2
- [27] Karan Singhal, Shekoofeh Azizi, Tao Tu, S. Sara Mahdavi, Jason Wei, Hyung Won Chung, Nathan Scales, Ajay Tanwani, Heather Cole-Lewis, Stephen Pfohl, Perry Payne, Martin Seneviratne, Paul Gamble, Chris Kelly, Abubakr Babiker, Nathanael Schärli, Aakanksha Chowdhery, Philip Mansfield, Dina Demner-Fushman, Blaise Agüera y Arcas, Dale Webster, Greg S. Corrado, Yossi Matias, Katherine Chou, Juraj Gottweis, Nenad Tomasev, Yun Liu, Alvin Rajkomar, Joelle Barral, Christopher Semturs, Alan Karthikesalingam,

- and Vivek Natarajan. Large language models encode clinical knowledge. *Nature*, 620(7972):172–180, 2023. 1
- [28] Louis Soum-Fontez, Jean-Emmanuel Deschaud, and François Goulette. Mdt3d: Multi-dataset training for lidar 3d object detection generalization. In *2023 IEEE/RSJ International Conference on Intelligent Robots and Systems (IROS)*, pages 5765–5772, 2023. 2, 3
- [29] Pei Sun, Henrik Kretschmar, Xerxes Dotiwalla, Aurelien Chouard, Vijaysai Patnaik, Paul Tsui, James Guo, Yin Zhou, Yuning Chai, Benjamin Caine, Vijay Vasudevan, Wei Han, Jiquan Ngiam, Hang Zhao, Aleksei Timofeev, Scott Ettinger, Maxim Krivokon, Amy Gao, Aditya Joshi, Yu Zhang, Jonathon Shlens, Zhifeng Chen, and Dragomir Anguelov. Scalability in perception for autonomous driving: Waymo open dataset. In *2020 IEEE/CVF Conference on Computer Vision and Pattern Recognition, CVPR 2020, Seattle, WA, USA, June 13-19, 2020*, pages 2443–2451. Computer Vision Foundation / IEEE, 2020. 3
- [30] Larissa T. Triess, Mariella Dreissig, Christoph B. Rist, and Johann Marius Zöllner. A survey on deep domain adaptation for lidar perception. *2021 IEEE Intelligent Vehicles Symposium Workshops (IV Workshops)*, pages 350–357, 2021. 1
- [31] Darren Tsai, Julie Stephany Berrio, Mao Shan, Eduardo Nebot, and Stewart Worrall. Ms3d++: Ensemble of experts for multi-source unsupervised domain adaptation in 3d object detection. *IEEE Transactions on Intelligent Vehicles*, pages 1–16, 2024. 3
- [32] TuSimple, Inc. Tusimple: Self-driving technology for long-haul freight. <https://www.tusimple.com/>, 2025. Accessed: 2025-05-10. 1
- [33] Yan Wang, Xiangyu Chen, Yurong You, Li Erran, Bharath Hariharan, Mark Campbell, Kilian Q. Weinberger, and Wei-Lun Chao. Train in germany, test in the usa: Making 3d object detectors generalize. In *Proceedings of the IEEE/CVF Conference on Computer Vision and Pattern Recognition*, pages 11713–11723, 2020. 3
- [34] Yan Wang, Junbo Yin, Wei Li, Pascal Frossard, Ruigang Yang, and Jianbing Shen. Ssda3d: Semi-supervised domain adaptation for 3d object detection from point cloud. In *Proceedings of the AAAI Conference on Artificial Intelligence*, 2023. 3
- [35] Zhenyu Wang, Yali Li, Hengshuang Zhao, and Shengjin Wang. One for all: Multi-domain joint training for point cloud based 3d object detection. In *Advances in Neural Information Processing Systems*, 2024. 3
- [36] Waymo LLC. Waymo: Autonomous driving technology company. <https://waymo.com/>, 2025. Accessed: 2025-05-09. 1
- [37] WeRide Inc. Weride - leading autonomous driving company. <https://www.weride.ai/>, 2025. Accessed: 2025-05-10. 1
- [38] Maciej K. Wozniak, Mattias Hansson, Marko Thiel, and Patric Jensfelt. Uada3d: Unsupervised adversarial domain adaptation for 3d object detection with sparse lidar and large domain gaps. *arXiv preprint arXiv:2403.17633*, 2024. 3
- [39] Guile Wu, Tongtong Cao, Bingbing Liu, Xingxin Chen, and Yuan Ren. Towards universal lidar-based 3d object detection by multi-domain knowledge transfer. In *Proceedings of the IEEE/CVF International Conference on Computer Vision (ICCV)*, pages 8669–8678, 2023. 3
- [40] Chao Xu, Chenghao Liu, Yuwei Liu, Yuntao Li, Xinyu Chen, Zhi Zhou, Junchi Zhang, Ming Yang, Qiang Yu, and Hao Tang. Revisiting domain-adaptive 3d object detection by reliable, diverse and class-balanced pseudo-labeling. In *Proceedings of the IEEE/CVF International Conference on Computer Vision (ICCV)*, pages 17141–17151, 2023. 3
- [41] Qiangeng Xu, Yin Zhou, Weiyue Wang, Charles R. Qi, and Dragomir Anguelov. Spg: Unsupervised domain adaptation for 3d object detection via semantic point generation. In *Proceedings of the IEEE/CVF International Conference on Computer Vision (ICCV)*, pages 15446–15456, 2021. 3
- [42] Yan Yan, Yuxing Mao, and Bo Li. Second: Sparsely embedded convolutional detection. *Sensors (Basel, Switzerland)*, 18, 2018. 2, 4
- [43] Binh Yang, Wenjie Luo, and Raquel Urtasun. Pixor: Real-time 3d object detection from point clouds. *2018 IEEE/CVF Conference on Computer Vision and Pattern Recognition*, pages 7652–7660, 2018. 2
- [44] Hongyang Yang, Xiao-Yang Liu, and Christina Dan Wang. Fingpt: Open-source financial large language models, 2023. 1
- [45] Jihan Yang, Shaoshuai Shi, Zhe Wang, Hongsheng Li, and Xiaojuan Qi. St3d: Self-training for unsupervised domain adaptation on 3d object detection. In *Proceedings of the IEEE/CVF Conference on Computer Vision and Pattern Recognition*, 2021. 3
- [46] Jihan Yang, Shaoshuai Shi, Zhe Wang, Hongsheng Li, and Xiaojuan Qi. St3d++: Denoised self-training for unsupervised domain adaptation on 3d object detection. *IEEE Transactions on Pattern Analysis and Machine Intelligence*, 2022. 3
- [47] Zetong Yang, Yanan Sun, Shu Liu, and Jiaya Jia. 3dssd: Point-based 3d single stage object detector. *2020 IEEE/CVF Conference on Computer Vision and Pattern Recognition (CVPR)*, pages 11037–11045, 2020. 2
- [48] Tianwei Yin, Xingyi Zhou, and Philipp Krähenbühl. Center-based 3d object detection and tracking. *CVPR*, 2021. 2, 4
- [49] Jiakang Yuan, Bo Zhang, Xiangchao Yan, Tao Chen, Botian Shi, Yikang Li, and Yu Qiao. Bi3d: Bi-domain active learning for cross-domain 3d object detection. In *Proceedings of the IEEE/CVF Conference on Computer Vision and Pattern Recognition (CVPR)*, pages 1497–1507, 2023. 3
- [50] Jiakang Yuan, Bo Zhang, Kaixiong Gong, Xiangyu Yue, Botian Shi, Yu Qiao, and Tao Chen. Reg-tta3d: Better regression makes better test-time adaptive 3d object detection. In *ECCV*, pages 197–213, 2024. 3, 6
- [51] Weichen Zhang, Wen Li, and Dong Xu. Srdan: Scale-aware and range-aware domain adaptation network for cross-dataset 3d object detection. In *Proceedings of the IEEE/CVF Conference on Computer Vision and Pattern Recognition (CVPR)*, pages 6769–6779, 2021. 3
- [52] Wayne Xin Zhao, Kun Zhou, Junyi Li, Tianyi Tang, Xiaolei Wang, Yupeng Hou, Yingqian Min, Beichen Zhang, Junjie Zhang, Zican Dong, Yifan Du, Chen Yang, Yushuo Chen, Zhipeng Chen, Jinhao Jiang, Ruiyang Ren, Yifan Li, Xinyu

- Tang, Zikang Liu, Peiyu Liu, Jian-Yun Nie, and Ji-Rong Wen. A survey of large language models, 2025. [1](#)
- [53] Yin Zhou and Oncel Tuzel. Voxelnet: End-to-end learning for point cloud based 3d object detection. *2018 IEEE/CVF Conference on Computer Vision and Pattern Recognition*, pages 4490–4499, 2017. [2](#)
- [54] Zoox, Inc. Zoox: Purpose-built autonomous mobility. <https://zoox.com/>, 2025. Accessed: 2025-05-09. [1](#)

Domain Adaptation for Different Sensor Configurations in 3D Object Detection

Supplementary Material

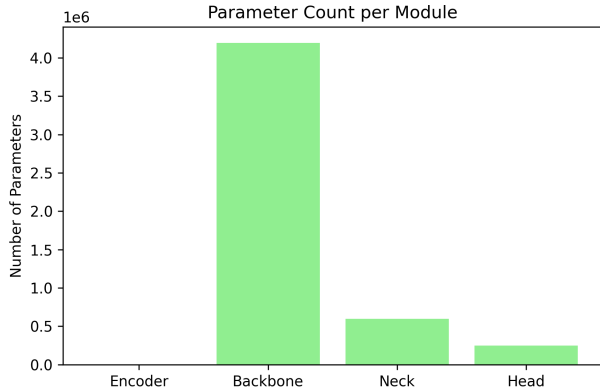


Figure 3. The total number of parameters for each layer.

6. Fine-tuning in Large Language Models

Fine-tuning has traditionally been used in various tasks not only in academia but also in industry. Recently, with the rapid development of large language models (LLMs) [17, 52], fine-tuning techniques themselves have also evolved. After pre-training base models on general natural language data (e.g. GPT [4, 19] or LLaMA [1, 2]), numerous efforts have been made to adapt these models to specific downstream tasks. For example, LLaMA-2 has been fine-tuned via supervised fine-tuning (SFT) to create models like LLaMA-2-chat that can follow user prompts; such models are often referred to as instruction-tuned models. There are also domain-specific fine-tuned models that are optimized for particular fields such as medicine and finance — for instance, Med-PaLM for medical [27], or FinGPT [44] for finance. These developments have brought renewed attention to the use of fine-tuning as a method for specialization. This study is inspired by such fine-tuning tasks in the LLM domain.

7. Additional analysis for fine-tuning

7.1. The Total Number of Parameters

We first examined the total number of parameters in the model. The parameter count for each architectural module is as follows:

- Encoder: 1,360 parameters
- Backbone: 4,194,304 parameters
- Neck: 599,552 parameters
- Head: 248,527 parameters

We illustrate this in Figure 3. This breakdown provides

Algorithm 1: Compute Layer-wise Parameter Difference

Input : Base model parameters \mathcal{B} , Target model parameters \mathcal{T} ,
Mode flag *is_relative* (boolean)

Output: Layer-wise L1 difference \mathcal{D} for each module

Initialize

$\mathcal{D}_{\text{diff}}[\text{Encoder, Backbone, Neck, Head}] \leftarrow 0.0$

Initialize

$\mathcal{D}_{\text{sum}}[\text{Encoder, Backbone, Neck, Head}] \leftarrow 0.0$

foreach parameter name $k \in \mathcal{B}$ **do**

if $k \in \mathcal{T}$ **and** $\mathcal{B}[k]$ is floating point **then**

$l \leftarrow \text{CategorizeLayer}(k)$

$\delta \leftarrow \|\mathcal{B}[k] - \mathcal{T}[k]\|_1$

$s \leftarrow \|\mathcal{B}[k]\|_1$

$\mathcal{D}_{\text{diff}}[l] \leftarrow \mathcal{D}_{\text{diff}}[l] + \delta$

$\mathcal{D}_{\text{sum}}[l] \leftarrow \mathcal{D}_{\text{sum}}[l] + s$

foreach layer type l in

 {Encoder, Backbone, Neck, Head} **do**

if *is_relative* = True **and** $\mathcal{D}_{\text{sum}}[l] > 0$ **then**

$\mathcal{D}[l] \leftarrow \mathcal{D}_{\text{diff}}[l] / \mathcal{D}_{\text{sum}}[l]$; ▷ Relative difference

else

$\mathcal{D}[l] \leftarrow \mathcal{D}_{\text{diff}}[l]$; ▷ Absolute difference

return \mathcal{D}

a structural understanding of where the model’s capacity is concentrated and serves as a basis for interpreting the magnitude of parameter differences across modules.

7.2. Analysis methods

To analyze parameter-level changes across model components, we compute the L1 difference between two sets of model weights. Algorithm 1 illustrates the procedure for calculating the layer-wise parameter differences. The algorithm first categorizes each parameter into one of four architectural modules: Encoder, Backbone, Neck, or Head, based on the parameter name. For each matched parameter between the two models, we compute the L1 distance and accumulate both the absolute difference and the L1 norm of the original parameter values. The final output can be computed in two modes.

- Relative difference: the accumulated L1 difference is normalized by the L1 norm of the original parameters, yield-

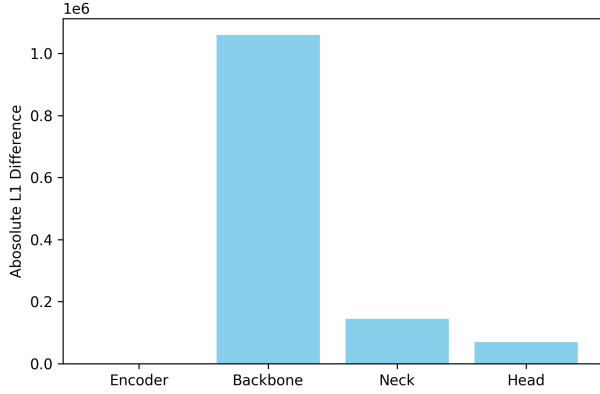


Figure 4. The absolute parameter differences between the RoboTaxi model and the RoboBus model.

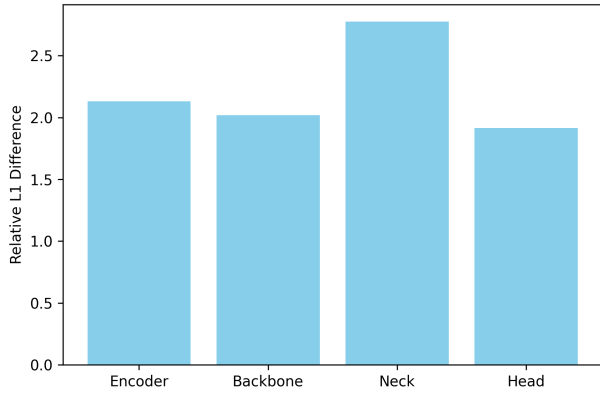


Figure 5. The relative parameter differences between the RoboTaxi model and the RoboBus model.

ing a scale-invariant measure.

- Absolute difference: the accumulated raw L1 difference is returned, which reflects the total magnitude of change regardless of scale.

The computation mode is controlled via a boolean flag `is_relative`. When set to `True`, the algorithm returns relative differences; otherwise, absolute values are used. This flexibility allows for analyzing both raw parameter shifts and their proportional impacts, depending on the application context.

7.3. Analysis Results

To better understand how different modules are affected by domain shift and training regimes, we analyzed the parameter differences across models. We first examined the absolute parameter differences between the RoboTaxi model and the RoboBus model. As shown in Figure 4, the differ-

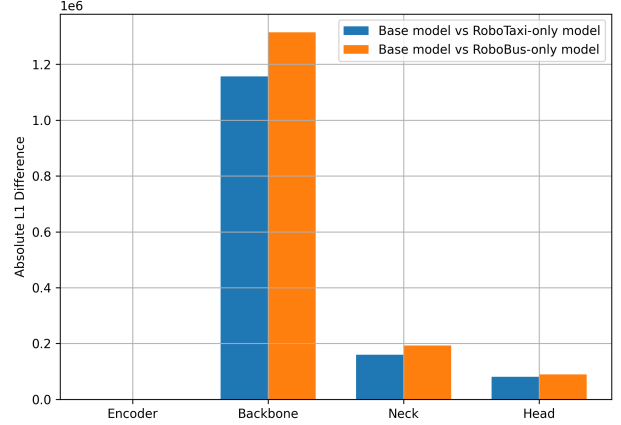


Figure 6. The absolute differences between the base model and RoboTaxi model, and between the base model and RoboBus model.

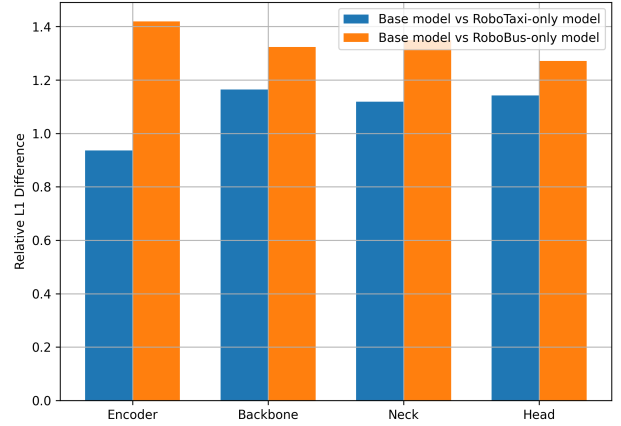


Figure 7. The relative differences between the base model and RoboTaxi model, and between the base model and RoboBus model.

ences across modules are largely proportional to the number of parameters each contains. This indicates that, in terms of raw magnitude, modules with more parameters naturally exhibit larger absolute shifts during training.

To remove the effect of parameter count and focus on proportional changes, we next analyzed the relative parameter differences between the same models, as shown in Figure 5. Interestingly, the Neck module shows the largest relative deviation, suggesting that it is most affected by the domain gap stemming from different sensor configurations. Since the Neck is responsible for aggregating multi-scale features from the backbone, this result implies that feature representation in this stage is particularly sensitive to sensor-induced variations.

We further examined the differences between the base model — obtained through joint training on both RoboTaxi and RoboBus datasets — and the domain-specific models. Figure 6 illustrates the absolute parameter differences between the base model and each of the domain-specific models. The RoboTaxi model is noticeably closer to the base model in absolute terms, which can be attributed to the fact that the RoboTaxi dataset contributes a greater number of frames to the joint training process. As a result, the base model is more strongly influenced by RoboTaxi data during optimization.

Relative differences between the base model and each of the domain-specific models are presented in Figure 7. These results further confirm that the RoboTaxi model remains closer to the base model, not only in absolute terms but also when normalized by parameter magnitude. The Encoder module shows the largest relative deviation, which can be explained by its small parameter count — minor changes have a disproportionately large effect on the relative metric. Conversely, the Head module shows the smallest relative change, suggesting that object categories and prediction structures are shared across domains. This implies that the domain gap caused by sensor configuration primarily affects early to mid-level representations, while the output space remains relatively stable.